Chinese Chemical Letters 37 (2026) 111942

Contents lists available at ScienceDirect

Chinese Chemical Letters

journal homepage: www.elsevier.com/locate/cclet

Deep eutectic solvent-mediated local delivery of Cacumen Platycladi essential oil against androgenetic alopecia

Dingmei Zhang[a,b,1], Yaping Liu[a,b,1], Sirui Liu[b], Jun Wu[c,*], Zhenfeng Wu[a,d,*], Wei He[a,b,*]

[a] Key Laboratory of Modern Preparation of Traditional Chinese Medicine (TCM), Ministry of Education, Jiangxi University of Chinese Medicine, Nanchang 330004, China
[b] School of Pharmacy, China Pharmaceutical University, Nanjing 211198, China
[c] Department of Geriatric Cardiology, Jiangsu Provincial Key Laboratory of Geriatrics, The First Affiliated Hospital of Nanjing Medical University, Nanjing 210029, China
[d] State Key Laboratory for the Modernization of Classical and Famous Prescriptions of Chinese Medicine, Nanchang 330004, China

ARTICLE INFO

Article history:
Received 22 July 2025
Revised 8 October 2025
Accepted 9 October 2025
Available online 10 October 2025

Keywords:
Androgenetic alopecia
Deep eutectic solvents
Essential oil
Transdermal delivery
Hair regeneration

ABSTRACT

Androgenetic alopecia (AGA) is the most common type of hair loss in clinical practice. Currently, the approved clinically used regimens for the treatment of alopecia include topical administration of minoxidil and oral finasteride. However, the two treatment approaches always demonstrate adverse effects and safety concerns. In the study, an aqueous transdermal delivery system (AqEDs) of Cacumen Platycladi essential oil (EO) was developed for the treatment of AGA, using deep eutectic solvent (DES) to solubilize the complex components of EOs. The AqEDs can stabilize EOs and allows transdermal delivery through lipid extraction with keratin conformational changes. AqEDs induced more significant hair regrowth effects in AGA model mice at a lower dosing frequency compared to minoxidil. This study potentially provides a safer and more effective strategy for the treatment of AGA.

© 2026 Published by Elsevier B.V. on behalf of Chinese Chemical Society and Institute of Materia Medica, Chinese Academy of Medical Sciences.

Androgenetic alopecia (AGA), also referred to as seborrheic alopecia, is a progressive condition marked by the gradual reduction of hair density and follicular miniaturization, predominantly in the frontal and vertex scalp regions [1–3]. As the most prevalent form of alopecia [4], AGA significantly impairs patients' psychosocial well-being and quality of life, despite lacking direct physical health risks [5,6]. The etiology of AGA involves multifactorial mechanisms, with excessive androgen sensitivity and dysregulated androgen metabolism implicated in over 90% of cases [7]. Emerging evidence suggests that modulating the follicular microenvironment or enhancing perifollicular angiogenesis may offer promising therapeutic avenues for AGA intervention [2,8,9]. The U.S. Food and Drug Administration (FDA) has approved minoxidil (MXD) and finasteride (FIN) for AGA treatment [10]. However, their clinical utility is limited by adverse effects such as contact dermatitis, hypertrichosis, and sexual dysfunction [11]. Consequently, natural compounds, including *Polygonum multiflorum* extract, *Panax ginseng* oil, and quercetin, have garnered attention as alternative therapies due to their favorable safety profiles and demonstrated hair-regrowth potential [12]. Nevertheless, their application face challenges, including poor follicular targeting, systemic side effects, and suboptimal efficacy [13]. As a result, developing a new strategy to improve their efficacy is designed.

The essential oil (EO) derived from Cacumen Platycladi (CP) is a volatile secondary metabolite composed of numerous bioactive compounds [14], exhibiting multi-target pharmacological properties, including anti-inflammatory, antioxidant, antimicrobial, and hair-regenerative effects [15]. These activities enable it to be a promising candidate for the prevention and management of AGA *via* synergistic mechanisms. For instance, CP EO has demonstrated 5α-reductase type 2 (SRD5A2) inhibitory activity [16], while topical application of the EO (0.2 g/kg) significantly extended the anagen phase in C57BL/6 mice, outperforming 2% minoxidil in promoting hair regrowth [17]. Cedrol, a major constituent of the EO, enhances perifollicular vascularization, thereby improving oxygen and nutrient supply to hair follicles [18]. Despite its therapeutic potential, like other EOs, the use of CP EO face challenges due to their inherent volatility, poor aqueous solubility, photothermal instability, and strong odor [19–21]. Moreover, as concentrated plant extracts, the EOs contain active ingredients at approximately 100-fold higher concentrations than their raw botanical sources [22]. Always, the EOs are dissolved in carrier oils or organic solvents for topical use, leading to cutaneous irritation, allergic reactions, and poor patient

* Corresponding authors.
E-mail addresses: wujun9989@njmu.edu.cn (J. Wu), zfwu527@163.com (Z. Wu), weihe@cpu.edu.cn (W. He).
[1] These authors contributed equally to this work.

https://doi.org/10.1016/j.cclet.2025.111942
1001-8417/© 2026 Published by Elsevier B.V. on behalf of Chinese Chemical Society and Institute of Materia Medica, Chinese Academy of Medical Sciences.

compliance [23]. Drug-carrier encapsulation technologies, such as, liposomes, emulsion systems (nanoemulsions, microemulsions) and nanocapsules could improve the EO stability [24–26]; however, the scale-up preparation is challenging and demonstrate high cost. Consequently, new approaches are still required to address the limitations, such as stability, bioavailability, and tolerability.

Deep eutectic solvents (DESs) are a class of low eutectic mixtures formed by the combination of hydrogen bond acceptors (HBAs) and hydrogen bond donors (HBDs) in specific stoichiometric ratios [27,28]. Their physicochemical properties, including solubilization capacity and percutaneous permeability, can be precisely tailored by varying the HBA/HBD composition [29,30]. Choline (Ch) is a biocompatible quaternary ammonium compound widely found in liver and cell membrane phospholipids [31]; geranic acid (Ge) is a natural monoterpene carboxylic acid commonly found in essential oils of cardamom, lemongrass, *etc.* [32]. Ch and Ge are both Generally Recognized as Safe (GRAS) ingredients [33]. The unique structure and molecular flexibility of Ch-Ge DES allows superior encapsulation of hydrophilic and lipophilic active agents, controlled release, and targeted delivery [34]. Moreover, the Ch-Ge DES system represents the first DES-based delivery platform to advance into clinical trials, currently under investigation for rosacea therapy [35]. Additionally, Ch-Ge DES exhibits superior biocompatibility and biodegradability and is attractive options for transdermal delivery [30].

In this study, we developed an aqueous EO-DES delivery system (AqEDs) of CP EO using DES as the transdermal carrier. AqEDs could efficiently encapsulate EO, promote its transdermal penetration through the unique solubilization property of DES, and significantly enhance its activity in promoting hair regeneration. Compared with the clinically used medicine (minoxidil), AqEDs is administered less frequently, with faster hair regrowth and better quality of regrown hair.

To prepare and characterize AqEDs, we first performed a compositional analysis of the EO. The total ion flow chromatogram obtained showed that about 55 compounds were isolated (Fig. S1 in Supporting information). Combined with the NIST 20.L spectral library search, a total of 31 compounds were identified (Table S1 in Supporting information). The results showed that the compounds with relatively high content in CP EO included α-pinene, sabinene, β-myrcene, 3-carene, D-limonene and γ-terpinene, *etc.*, while the main constituents were monoterpenes and sesquiterpenoids. As a result, the CP EO demonstrate the properties, including low solubility, high volatility, photothermal instability, irritation, release, *etc.* [36].

Next, we prepared DES by heating method [37] using Ch and Ge in a 1:2 molar ratio [36]. DES was a yellow transparent viscous liquid at indoor temperature with moderate fluidity and characteristic odor, and the density of DES was 0.97 ± 0.01 g/mL, the viscosity was 646 ± 45 mPa·s, and the conductivity was 11.56 ± 0.65 ms/m, consistent with the previous report [32]. To characterize the DES synthesis, we performed the structural analysis was performed using proton nuclear magnetic resonance spectroscopy (^{1}H-NMR) and nuclear overhauser effect spectroscopy (NOESY). The structures of Ge and Ch are shown in Fig. 1A, with the corresponding protons labeled on the spectra. The two terminal methyl groups of Ge (labeled 9 and 10) appear first at 1.56 and 1.63 ppm, followed by the internal methyl group and the CH_2 group (labeled 5, 6, and 11) at 2.02 ppm. Methyl groups (5, 6, and 7) attached to the Ch nitrogen atom appear at 3.19 ppm, and protons (3 and 2) on the Ch hydroxyl chain are located at 3.46 and 3.86 ppm, respectively. The protons (7 and 3) attached to the sp^2 carbon on Ge appear at 5.08 and 5.61 ppm. In addition, strong hydrogen bonding interactions were formed between the carboxyl group of Ge and the hydroxyl group of Ch, which promoted rapid proton exchange and led to the neutralization of the acidic protons in Ge [38]. The

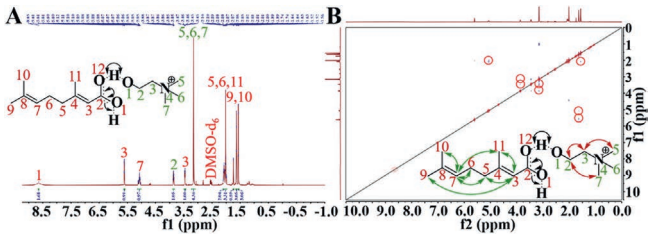


Fig. 1. Characterization of DES. (A) ^{1}HNMR spectroscopy of DES. Inset shows the structure of Ge and Ch components. The numbering of the peaks reflects the assignation of the protons of each molecule to the measured signal. (B) NOESY spectrogram of DES, showing the through space interactions circled for DES. The red circles indicate cross peaks The red and green arrows mark the NOE correlation signals between different hydrogen protons, indicating the spatial proximity between the corresponding protons; the black arrows indicate the proton exchange kinetic processes in the system.

results confirmed the synthesis of the DES system. Then, NOESY was employed to further analyze the intra-ion interactions. The isophase crossing peaks are bracketed by circles, indicating two groups of protons within 5 Å of each other. As shown in Fig. 1B, a total of eight cross peaks were observed, indicating the existence of two sets of proton pairs with spatial distances <5 Å, with strong spatial proximity effects. Collectively, Ch and Ge in the DES system could bind together through multiple noncovalent interactions, forming a stable three-dimensional supramolecular structure.

DESs have self-assembling behavior in water and form colloidal systems, such as micelles or emulsions, due to the hydrophilic of Ch and hydrophobic tails of Ge [39,40]. The micellar structure can increase skin permeability through diffusion and fusion during transdermal drug delivery [30]. The hydrogen bonding allowed the DES to dissolve EOs; then, the predominant interaction forces, such as $\pi-\pi$ stacking and hydrogen bonding, motivated the EO-DES to assemble into nanosized structures in aqueous conditions [36]. The inherent three-dimensional hydrogen-bonded network structure of DES effectively adsorbs complex components within EO, thereby enhancing the stability of the EO-DES system against water dilution or physical disruption. Moreover, water dilution reduces the EO-DES preparation's viscosity, greasiness, and irritation of EOs, improving the topical delivery [41]. Here, we prepared AqEDs by adding the EO to DES, vortexing and water dilution. The optimal prescriptions of homogeneous and stable AqEDs were screened using polydispersity index (PDI) as the key evaluation index (Table S2 in Supporting information). The PDI of 0.5%, 1% and 2% AqEDs were all <0.3, indicating a narrow size distribution (Fig. 2A). As shown in Fig. 2B and Table S3 (Supporting information), the three formulations demonstrated the separation percentage (SP) values of 0 and <0.3 PDI values after centrifugation. The results indicated that the AqEDs had promising centrifugal stability. Moreover, the content of α-pinene, a main constituent in EO, in the formulations displayed little alteration after the influence factor test (Figs. 2C and D) and accelerated- (Fig. 2E) and long-term studies (Fig. 2F). The data indicated that AqEDs had promising storage stability.

To study the transdermal permeability of formulations, we prepared fluorescein isothiocyanate (FITC)-labeled AqEDs and performed *in vitro* and *in vivo* transdermal experiments. The permeation within 0.5–12 h conformed to the zero-level kinetic model (Fig. 2G, Fig. S3 and Table S4 in Supporting information). The FITC permeability from AqEDs was significantly improved compared to the phosphate-buffered saline (PBS) and was concentration dependent. Furthermore, the dye retention in the AqEDs group was higher than that in the control group (Fig. 2H and Fig. S3). Moreover, AqEDs demonstrated significantly stronger fluorescence in the dermis compared to PBS (Figs. 2I and J). As a result, AqEDs could effectively penetrate the SC and transport drugs to the dermis.

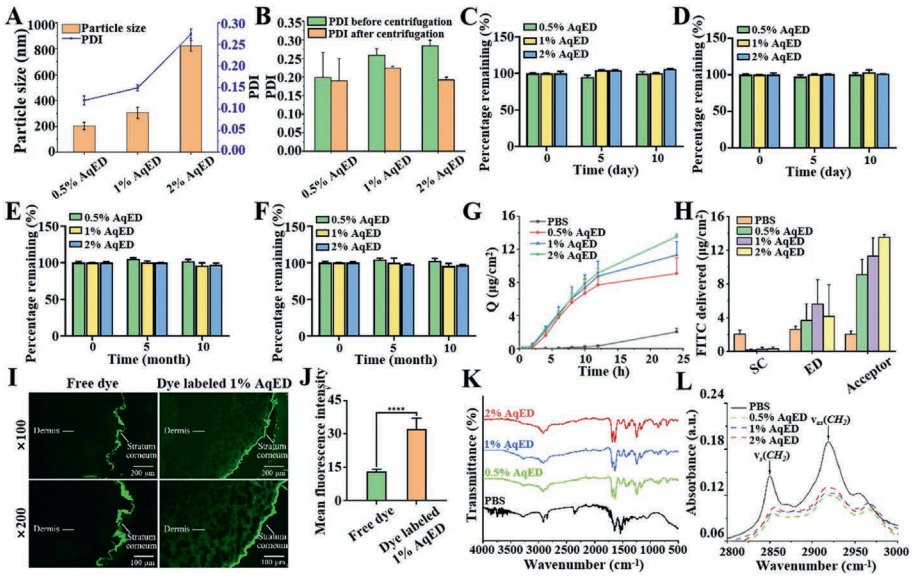


Fig. 2. Preparation and characterization of AqEDs. (A) Homogeneity experiment. (B) Centrifugal stability. (C) High temperature test. At the high temperature of 60 °C, the AqEDs were stored for 0, 5 and 10 days and analyzed for the content of α-pinene in the EO. (D) Srong light exposure test. Under the illumination conditions of 25 °C and 4500 ± 500 LX, the AqEDs were stored for 0, 5 and 10 days and analyzed for the content of α-pinene. (E) Accelerated test At 40 ± 2 °C, 75 % ± 5 % accelerated test conditions, the AqEDs were stored for 0, 1 and 3 months and analyzed for the content of α-pinene. (F) Long-term test. At a constant temperature and humidity of 25 ± 2 °C and 60 % ± 5 %, the AqEDs were stored for 0, 1 and 3 months and analyzed for the content of α-pinene. (G) *In vitro* transdermal absorption ($n = 3$). (H) Distribution of FITC retention at different sites ($n = 3$). SC: stratum corneum; ED: epidermis and dermis. (I) *In vitro* transdermal fluorescence observation. Scale bar: 200, 100 μm. (J) emiquantitative analysis of fluorescence intensity ($n = 3$). Data are presented as mean ± standard deviation (SD). $^{****}P < 0.0001$. (K) Attenuated total reflection FTIR (ATR-FTIR) scanning spectra of stratum corneum before and after treatment with the preparation. (L) ATR-FTIR spectra of key molecular vibrational features of the transdermal mechanism of the AqEDs.

Next, we studied the transdermal mechanism according to the previously reported method [32,42]. FITC, a classical fluorescent marker for transdermal drug delivery studies, has molecular properties similar to those of the active ingredients in EOs and has excellent fluorescent stability [43]. As shown in Fig. S2 (Supporting information), the SC slices were intact and had tightly arranged keratinocytes in a scale-like pattern. Compared with the PBS-treated SC slices, after treatment with the AqEDs, the peak areas at 2850 and 2920 cm^{-1} decreased, and the mobility of the lipid structure of SC increased (Fig. 2L). Ge, which is more predominant in DES, is highly hydrophobic and is capable of extracting lipids from SC and allowing DES to penetrate into the lipid extraction region [44]. The lipid arrangement of SC was altered, allowing the drug penetration into the skin. In addition, the treated SC demonstrated the peak split at 1645.2 cm^{-1} (amide I band) and a double peak (Fig. 2K), implying that the change of the keratin conformation and the increased disordered structure [45,46]. The results suggest that lipid extraction and keratin conformation change are the key mechanisms for AqEDs to improve transdermal delivery.

Finally, we studied the hair regeneration-promoting effect of the preparations using an AGA mouse model [8,47], using commercialized minoxidil as a positive control. The indicators included the quality of newborn hair, the rate of follicular cycle transition, and perifollicular vascular neovascularization. All experimental procedures were performed according to the protocols approved by China Pharmaceutical University Institutional Animal Care and Use Committee (No. 202407082).

The establishment of the AGA mouse model was mapped out in Fig. S4 (Supporting information). The treatment using 0.2 % (w/v) testosterone partially inhibited the conversion of hair follicles from the resting to the growing phase compared to the control (non-treatment). The hair follicle regeneration was significantly inhibited in the 0.5 % testosterone model group. Here, the AGA mouse model was constructed by topically dosing 0.5 % (w/v) testosterone solution.

The 21-day treatment using preparations demonstrated profound hair regeneration compared to the model group (Figs. 3A and B). While the time of skin darkening in the 2 % AqED group was significantly earlier than other groups (Fig. 3C), promoting resting phase of hair follicles into the anagen phase.

The hair follicles on day 14 in the 0.5 %, 1 % AqED and minoxidil groups were activated from the resting phase and entered the anagen I-IIIa stage; in the 2 % AqED group, the clear hair shaft structure could be observed, which indicated that the hair follicles had entered the anagen IIIb-IIIc stage (Fig. 3D). Moreover, the percentage of anagen follicles in the 2 % AqED group was significantly higher than other groups (Fig. 3E). In addition, the treatment using 2 % AqED demonstrated highest promotion (Fig. 3F). The results indicated that 2 % AqED significantly accelerated the conversion process of hair follicles from resting phase to anagen phase and was comparable to the clinically used drug (minoxidil).

Then, cell proliferation during the follicular cycle transition was examined. The treatment effect of AqEDs at day 14 post administration on the density of Ki67-positive cells in the hair bulb of hair follicles was concentration dependent (Figs. 3G and H). Again, 2 % AqED group indicated the most significant cell proliferation. The data suggested that AqED promoted the transition of hair follicles from resting to growing phase by activating the proliferation of hair follicle stem cells.

Lastly, we studied perifollicular neovascularization *via* determining the CD31 a specific marker for vascular endothelial cells that reflects the distribution of microvessels in tissues [48]. As shown in Fig. 3I, the strongest fluorescence intensity and profound activation of vascular endothelial cells was demonstrated in the 2 % AqED group. The CD31 expression in the 1 % AqED group was similar to the minoxidil group. The results indicated that AqEDs elevated CD31-positive vascular neovascularization in a concentration-dependent manner. Moreover, the 2 % AqED group demonstrated many mature blood vessels gathering below the hair follicles and mostly arranging in concentric circles and indicated greater lumen dilatation than the minoxidil group (Fig. 3J). As dis-

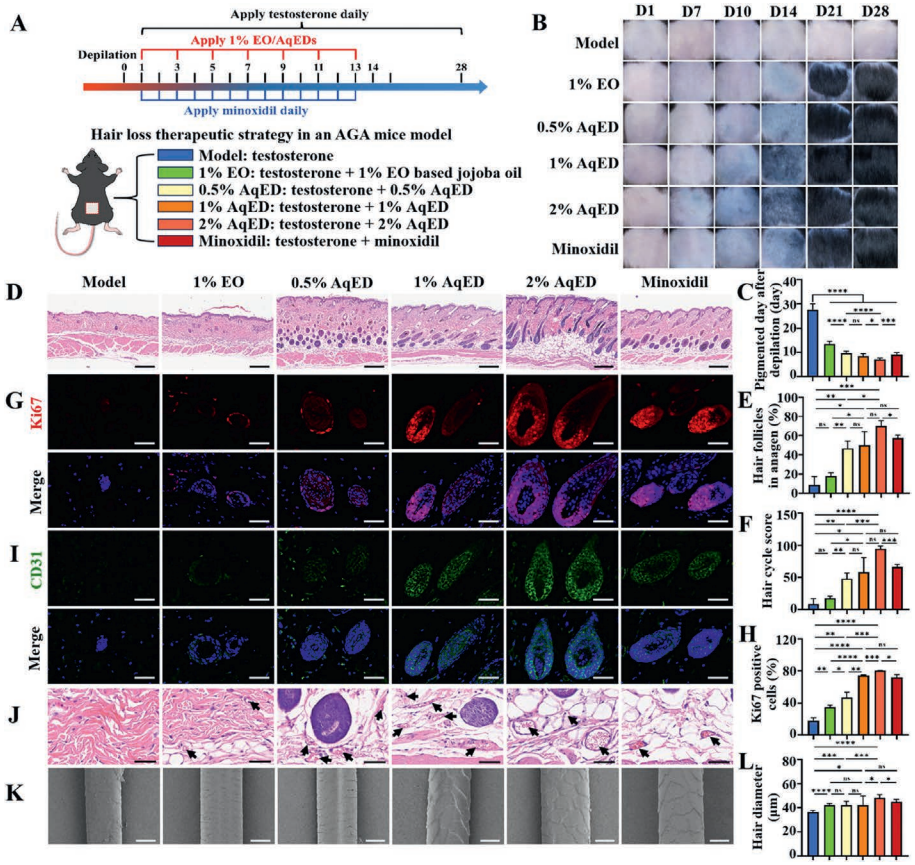


Fig. 3. *In vivo* treatment efficacy against AGA. (A) Dosing regimen and grouping for AGA mouse modeling. C57BL/6 mice (7 weeks old) were randomly divided into 6 groups according to body weight: model group, groups treated with 1 % EO, 0.5 % AqED, 1 % AqED or 2 % AqED, and the positive control group (minoxidil group). The model group was treated with 0.5 % (w/v) testosterone solution daily at a dosage of 0.1 mL cm^{-2} d^{-1} for 28 days; the minoxidil group was treated with 5 % (w/v) minoxidil solution daily at the same dosage as that of the model group on top of the model group's administration for 13 days; the other groups were treated with 20 μL 1 % EO solution (solvent of jojoba oil), 0.5 %, 1 %, and 2 % AqED preparations, respectively, every other day, on top of the model group's administration for 13 days. (B) Representative pictures of hair regeneration in each group of mice. (C) Time of skin pigmentation after hair removal ($n = 3$). (D) H&E staining graph of skin tissue on day 14 for studying the neovascularization around hair follicles. (E) Percentage of anagen follicles in total hair follicles ($n = 3$). (F) Day 14 follicular cycle score ($n = 3$). (G) Day 14 Ki67 immunofluorescence staining images. Red: Ki67 (proliferation marker). Scale bar: 50 μm. (H) Results of semi-quantitative analysis of Ki67 fluorescence intensity ($n = 3$). (I) Immunofluorescence staining map of CD31 in skin tissues for labeling vascular endothelial cells. Scale bar: 50 μm. (J) H&E staining image of skin tissue. Black arrows indicate skin vascular structures. Scale bar: 50 μm. (K) Representative scanning electron microscope (SEM) images of neonatal hairs of each group of mice. Scale bar: 20 μm. (L) Neonatal hairs diameters ($n = 9$). Data are presented as mean ± SD. ns, not statistically significant. $^{*}P < 0.05$, $^{**}P < 0.01$, $^{***}P < 0.001$, $^{****}P < 0.0001$.

played in Fig. 3K, the neonatal hairs in the groups treated with 1 %, 2 % or minoxidil were thicker with a complete hair-scale structure. 2 % AqED had a greater diameter of newborn hairs than the minoxidil group (Fig. 3L).

Collectively, the results indicated that AqED treatments significantly increased the weight and diameter of newborn hairs. At lower dosing frequencies, the AqEDs demonstrated therapeutic efficacy against AGA comparable to the clinically used minoxidil.

Additionally, we studied the safety of preparations. As shown in Fig. S5 (Supporting information), DESs indicate little cytotoxicity on HaCaT cells in the concentration range of 0–16 mg/mL. Then, we determined the topical skin thickness at 24 and 28 days after treatment. The treatment using 0.5 % and 2 % AqED demonstrated higher skin thickness than minoxidil group at day 14 and, while, indicated no significant difference compared with the model group at day 28 (Fig. S6 in Supporting information). This result confirmed the favorable *in vivo* safety of topical application of AqEDs.

To assess the skin irritation of the preparations, we stained the tissue sections by hematoxylin and eosin (H&E) staining. As shown in Fig. 4, the rat epidermis in the DES- and 2 % AqED-treated groups showed several alterations, such as the stratum corneum cell detachment, the thickening of the stratum corneum, and squamous epithelial hyperplasia. The atrophy of the dermal cells and inflammatory cell infiltration were observed in the dermis after

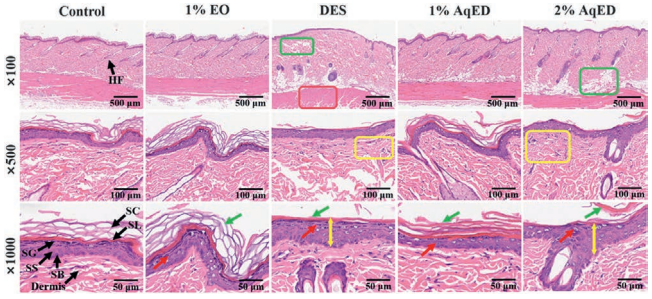


Fig. 4. H&E-stained sections of skin tissues in the administered area. The animals were topically administered continuously for 5 days. Control: saline. SC: stratum corneum, SL: stratum lucidum, SG: stratum granulosum, SS: stratum spinosum, SB: stratum basale, Dermis: dermis, HF: hair follicle. Green arrows: cuticle cell detachment; Yellow arrow: the thickening of the stratum corneum; Red arrows: squamous epithelial hyperplasia of the skin. Green box: dermal cell atrophy occurs in the dermis; Yellow box: inflammatory cell infiltration; Red box: subcutaneous tissue cell morphology changes from spindle to ellipsoid shape.

treatment. In addition, the cell morphology of the subcutaneous tissue in the DES group changed from a shuttle shape to an ellipsoid shape. The results are consistent with the previous report that the skin returns to the normal structure after discontinuing

use [33]. Currently, the Ch/Ge-based DES has advanced to the local application clinical research stage [33]. A Human Repeat Insult Patch Test (HRIPT) showed that this DES did not elicit a sensitization response and had minimal or acceptable skin irritation. As a result, AqEDs have a promising dermal safety profile under short-term, interval dosing conditions, providing an important safety rationale for their translational clinical use.

In this study, we developed the AqEDs for topical administration of CP EO using DES as the transdermal carrier and followed by aqueous dilution. The preparation could improve the topically transdermal delivery of the complex components in the EO, activate hair follicle stem cell proliferation and promote angiogenesis, improve the microenvironment of hair follicles, promote hair follicle regeneration, and ultimately achieve a promising effect against hair loss. More convincingly, compared with the clinical drug minoxidil, AqEDs is administered less frequently, with faster hair regrowth and better quality of regrown hair. This study provides rational evidence for the clinical application of AqEDs and a promising strategy for the treatment of AGA.

CRediT authorship contribution statement

Dingmei Zhang: Writing – review & editing, Writing – original draft, Conceptualization. **Yaping Liu:** Methodology, Investigation, Conceptualization. **Sirui Liu:** Methodology, Investigation. **Jun Wu:** Project administration, Investigation, Conceptualization. **Zhenfeng Wu:** Supervision, Funding acquisition, Conceptualization. **Wei He:** Writing – review & editing, Writing – original draft, Supervision, Conceptualization.

Declaration of competing interest

The authors declare that they have no known competing financial interests or personal relationships that could have appeared to influence the work reported in this paper.

Acknowledgments

This study was supported by the Key Laboratory of Modern Chinese Medicine Preparation of Ministry of Education of Jiangxi University of Traditional Chinese Medicine (No. zdsys-202103), and the Key R&D Plan of Ganjiang New District of Jiangxi (No. 2023010).

Supplementary materials

Supplementary material associated with this article can be found, in the online version, at doi:10.1016/j.cclet.2025.111942.

References

[1] S.L. Jing, Y.H. Liu, B. Wang, et al., J. Control. Release 381 (2025) 113597.
[2] A.R. Yuan, F. Xia, Q. Bian, et al., ACS Nano 15 (2021) 13759–13769.
[3] S.M. Perez, K.N. Williams, B. Nguyen, A. Tosti, JAAD Rev. 2 (2024) 81–87.
[4] L.P. Yuan, M. Pan, H.Z. Deng, et al., Chin. Chem. Lett. 36 (2025) 110723.
[5] C.C. Chou, P.C. Cheng, H.C. Chen, et al., J. Am. Acad. Dermatol. 91 (2024) AB119.
[6] M. Pereira-Silva, A.M. Martins, I. Sousa-Oliveira, et al., Acta Biomater. 142 (2022) 14–35.
[7] W.J. Yan, J.K. Liu, X.D. Xie, et al., Stem. Cell Res. Ther. 15 (2024) 439.
[8] Y.T. Yang, P. Wang, Y. Gong, et al., Theranostics 13 (2023) 3675–3688.
[9] J. Gao, Z.Z. Weng, Z. Zhang, et al., Adv. Healthc. Mater. 13 (2024) 2303095.
[10] S. Devjani, O. Ezemma, K.J. Kelley, E. Stratton, M. Senna, Drugs 83 (2023) 701–715.
[11] S. Salim, K. Kamalasanan, J. Control. Release 325 (2020) 84–99.
[12] S.Q. Wu, X.H. Kou, Y.J. Niu, et al., Eur. J. Med. Chem. 264 (2024) 116022.
[13] Y.T. Gu, Q. Bian, Y.J. Zhou, Q.L. Huang, J.Q. Gao, Asian J. Pharm. Sci. 17 (2022) 333–352.
[14] S. Khalid, K. Chaudhary, S. Amin, et al., Ultrason. Sonochem. 107 (2024) 106914.
[15] A.N.R. Corrêa, C.D. Ferreira, Crit. Rev. Food Sci. Nutr. 63 (2023) 8960–8974.
[16] B. Zhang, R.W. Zhang, X.Q. Yin, et al., J. Ethnopharmacol. 177 (2016) 1–9.
[17] Y. Zhang, S.S. Chen, F.Z. Qu, G.Y. Su, Y.Q. Zhao, J. Ethnopharmacol. 238 (2019) 111835.
[18] Y. Zhang, L. Han, S.S. Chen, et al., Biomed. Pharmacother. 83 (2016) 641–647.
[19] A.M. Bakry, S. Abbas, B. Ali, et al., Compr. Rev. Food Sci. Food Saf. 15 (2016) 143–182.
[20] K. Chen, M. Zhang, B. Bhandari, A.S. Mujumdar, Food Res. Int. 139 (2021) 109809.
[21] Q.L. Hao, H. Peng, R.C. Zhao, et al., Chin. Chem. Lett. 33 (2022) 320–323.
[22] H. Falleh, M. Ben Jemaa, M. Saada, R. Ksouri, Food Chem. 330 (2020) 127268.
[23] J.S. Raut, S.M. Karuppayil, Ind. Crops. Prod. 62 (2014) 250–264.
[24] X.T. Li, Y.Y. Lai, G.H. Wan, et al., Chin. J. Nat. Med. 22 (2024) 1100–1116.
[25] N. Lammari, O. Louaer, A.H. Meniai, A. Elaissari, Pharmaceutics 12 (2020) 431.
[26] M.R. Díaz, E.G. Hernández, B.G. Villanova, V. Verardo, Food Chem. 354 (2021) 129575.
[27] F.F. Ajayi, P. Mudgil, S. Maqsood, Food Chem. 484 (2025) 144262.
[28] W. He, Y.J. Shi, D. Qu, Chin. J. Nat. Med. 22 (2024) 1065–1066.
[29] J.L. Shamshina, R.D. Rogers, Chem. Rev. 123 (2023) 11894–11953.
[30] B. Xie, Q. Jiang, F. Zhu, et al., Chin. Chem. Lett. 36 (2025) 110508.
[31] S.H. Zeisel, K.C. Klatt, M.A. Caudill, Adv. Nutr. 9 (2018) 58–60.
[32] E.E.L. Tanner, K.N. Ibsen, S. Mitragotri, J. Control. Release 286 (2018) 137–144.
[33] S. Mitragotri, J. Control. Release 376 (2024) 593–600.
[34] M.K. Shukla, H. Tiwari, R. Verma, et al., Pharmaceutics 15 (2023) 702.
[35] J. Ko, A. Mandal, S. Dhawan, et al., Bioeng. Transl. Med. 6 (2021) 10191.
[36] Y.P. Liu, D. Wang, Y.Y. Lai, et al., Langmuir 40 (2024) 23766–23779.
[37] Y. Yan, L.Q. Shen, Y. Wang, et al., Chin. Chem. Lett. 36 (2025) 110845.
[38] M. Cherniakova, V. Varchenko, K. Belikov, Chem. Rec. 24 (2024) 202300267.
[39] M.N. Huda, I.G. Deaguero, E.A. Borrego, et al., J. Control. Release 349 (2022) 783–795.
[40] Y.J. Shi, Z.M. Zhao, Y.S. Gao, et al., J. Control. Release 322 (2020) 602–609.
[41] M. Nurunnabi, K.N. Ibsen, E.E.L. Tanner, S. Mitragotri, Proc. Natl. Acad. Sci. U. S. A. 116 (2019) 25042–25047.
[42] A. Banerjee, K. Ibsen, Y. Iwao, M. Zakrewsky, S. Mitragotri, Adv. Healthc. Mater. 6 (2017) 1601411.
[43] S. Kusama, K. Sato, Y. Matsui, et al., Nat. Commun. 12 (2021) 658.
[44] X.J. Chen, Z.Q. Li, C.R. Yang, D.G. Yang, Asian J. Pharm. Sci. 19 (2024) 100900.
[45] Q.M. Qi, S. Mitragotri, J. Control. Release 311-312 (2019) 162–169.
[46] E. Beaven, R. Kumar, J.M. An, et al., Adv. Drug Deliv. Rev. 204 (2024) 115157.
[47] D.L. Fu, J.F. Huang, K.T. Li, et al., Biomed. Pharmacother. 137 (2021) 111247.
[48] S.Y. Fu, F.H. Chen, C.C. Wang, et al., Int. J. Radiat. Oncol. Biol. Phys. 109 (2021) 1547–1558.